Performance of an Isobaric Hybrid Compressed Air Energy Storage System at Minimum Entropy Generation

Sammy Houssainy
National Renewable Energy Laboratory,
15013 Denver West Pkwy.,
Golden, CO 80401
e-mail: sammyhoussainy@ucla.edu

Mohammad Janbozorgi
Department of Mechanical and
Aerospace Engineering,
University of California, Los Angeles,
CA 46-147A Engineering IV,
Los Angeles, CA 90095-1597
e-mail: mjanbozorgi@gmail.com

Pirouz Kavehpour
Department of Mechanical and Aerospace
Engineering,
University of California, Los Angeles,
CA 46-147A Engineering IV,
Los Angeles, CA 90095-1597
e-mail: pirouz@seas.ucla.edu

Efficient, large-scale, and cost-effective energy storage systems provide a means of managing the inherent intermittency of renewable energy sources and drastically increasing their utilization. Compressed air energy storage (CAES) and its derivative architectures have received much attention as a viable solution; however, optimization objectives for these systems have not been thoroughly investigated in the literature. A hybrid thermal and compressed air energy storage (HT-CAES) system is investigated that mitigates the shortcomings of the otherwise attractive conventional CAES systems and its derivatives—shortcomings such as strict geological locations, low energy densities, and the production of greenhouse gas emissions. The HT-CAES system allows a portion of the available energy to operate a compressor and the remainder to be converted and stored in the form of heat through joule/resistive heating in a high-temperature, sensible, thermal energy storage medium. Internally reversible and irreversible HT-CAES system assumptions were investigated, in addition to regenerative and non-regenerative design configurations. Several system optimization criteria were examined—including maximum energy efficiency, maximum exergy efficiency, maximum work output, and minimum entropy generation—with a focus on whether the latter may lead to conclusive design guidelines in a real system. It is shown that an HT-CAES system designed based on a minimum entropy generation objective may operate at a lower energy and exergy efficiency as well as lower output power than otherwise achievable. Furthermore, optimization objective equivalence is shown to be limited to certain design conditions. [DOI: 10.1115/1.4045931]

Keywords: minimum entropy generation, compressed air energy storage, hybrid energy storage, CAES, energy storage, thermal energy storage, alternative energy sources, energy conversion/systems, energy storage systems, energy systems analysis, heat energy generation/storage/transfer, renewable energy

1 Introduction

Increased awareness of the detrimental environmental effects of fossil fuel emissions and rising concern over global warming are accelerating incentives to harness and integrate sustainable sources of energy in our existing infrastructure. However, our efforts to increase the integration of sustainable power are hindered by the challenges associated with the intermittency of these sources [1–6]. A logical solution is to incorporate large-scale energy storage systems, which would serve to store the low-quality (fluctuating) power supply and provide high-quality (smooth) and dispatchable power based on the demand [7–11].

Compared to chemical energy storage (batteries), mechanical energy storage systems—such as compressed air energy storage (CAES), pumped hydro storage (PHS), and flywheels—are generally capable of more cycles, have steady efficiencies, and are better suited for large-scale applications (with the exception of flywheels). However, among the mechanical systems, PHS requires specific geological locations and higher maintenance and capital costs as compared with CAES systems, rendering CAES most suitable for renewable integration [12–15].

Three types of CAES systems have been extensively investigated in the literature: diabatic (D-CAES), isothermal (I-CAES), and advanced adiabatic (AA-CAES) [16–21]. In conventional CAES, which is diabatic, the exergy associated with compression heat is not used, drastically hindering its performance. The only two existing CAES systems in the world are based on the diabatic method. Furthermore, natural gas is used as an external heat source, providing up to 60% of the total output energy, contingent on the fuel conversion efficiency. Therefore, D-CAES is more properly classified as a mutual power generation and energy storage system [22,23]. For these reasons, significant efforts have been devoted toward I-CAES and AA-CAES, which address the drawbacks of conventional CAES systems by avoiding the use of fossil fuels and enhancing compression performance.

Through high heat-transfer rates, I-CAES aims to isothermally compress and expand the air. I-CAES is advantageous because it minimizes compression work and eliminates the need for combustion emissions. However, its major drawback results from the exceedingly high storage pressures necessary for adequate energy densities [24–27]. Several methods have been proposed to achieve isothermal compression conditions. Hydro-pneumatic energy storage (HyPES) is one common type, where a liquid performs the air-compression process. Hydraulic oils are most commonly investigated in HyPES due to their high heat capacity and stability at high pressures [28,29]. Recent works investigate the spraying of water in a reciprocating piston to collect the generated heat of compression while minimizing the rise in air temperature. The warm water is then similarly used to minimize the drop-in air temperature during the expansion. Research and development efforts must be undertaken on such machinery that needs to tolerate moisture [30]. In addition to water, the foam has been investigated for enhanced heat transfer [31].

Another CAES derivative that also eliminates combustion emissions is the advanced adiabatic type. Unlike D-CAES, where the compression heat is wasted and natural gas combustion is used as a heat source, in AA-CAES, the compression heat is stored and reused as a heat source during the expansion. The simplest AA-CAES architecture, which reuses the compression heat, is achieved by storing the hot compressed air itself in a temperature-resilient air storage medium [32]. Alternatively, a common method is to store the heat separately in a thermal energy storage medium, which would require less thermally resistant air storage methods. The performance of AA-CAES with a separate thermal storage unit increases with storage temperature, as demonstrated by several investigations [33–39]. However, the low exhaust temperatures of available compressors in the market limit the performance and energy density of AA-CAES systems [19,40–45].

The hybrid thermal and compressed air energy storage (HT-CAES) system, presented in this paper, addresses the drawbacks of conventional and AA-CAES systems. Contrary to D-CAES and similar to AA-CAES, in HT-CAES, the combustion emissions are mitigated by using compression heat. However, unlike AA-CAES, the need for high-temperature compressors is eliminated by storing electrical power directly in the form of heat through Joule heating, reaching high temperatures prior to the expansion. Therefore, HT-CAES allows for both high energy densities and efficiencies. The separation of energy between thermal and compressed air energy storage allows for lower storage pressures and volume because the additional heat increases the capacity of the system. Consequently, increased flexibility associated with HT-CAES reduces geological restrictions. Although very few groups have investigated an HT-CAES concept [46,47], the isobaric storage volume condition presented here has not been examined in the literature. In addition, the optimization objectives of such a system have received no attention. Conversely, the optimization of heat engines is an old subject of thermodynamics [48–50]. Various optimization objectives have been examined to investigate the performance of standard power cycles such as Brayton, Otto, Diesel, Atkinson, Millar, and Dual cycles [51,52]. However, such analysis has not been employed on a hybrid thermal-compressed air energy storage system. The most common optimization criteria examined in the literature for power cycles are the maximum efficiency, maximum work output, minimum entropy generation, and maximum ecological function [53]. According to the Gouy-Stodola theorem, the maximum output power and minimum entropy production rate are equivalent. However, this equivalence in heat engines was later shown to be limited to certain design conditions. For heat engines, the maximum thermal efficiency and maximum work output do not necessarily coincide. For example, in a regenerative Brayton cycle, maximum work and maximum thermal efficiency coincide only at regenerator effectiveness of 50% [54]. Whether the optimization objective should be performed based on the maximum power or maximum efficiency depends on the application. However, in general, the operational regime should be between the maximum efficiency and maximum output power design points.

The main objective of this paper is to investigate the performance of an isobaric HT-CAES system at the point of minimum entropy generation—which, to the best of our knowledge, has not been reported previously. Both the energy and exergy efficiencies are examined, and the optimum design points leading to their maxima are compared with the design point corresponding to minimum entropy generation. The premise is to determine whether the minimization of entropy generation may lead to useful design recommendations. Additionally, a discussion is provided that demonstrates the criterion at which the maximum energy efficiency and maximum exergy efficiency become coincident with the design point of minimum entropy generation. Throughout the analysis, it is assumed that external irreversibilities are present. The effects of both internally reversible and irreversible processes are examined and compared. Additionally, the thermal energy storage efficiency is considered as well as its effects on

the optimum design points, leading to an examination of maximum energy efficiency, maximum exergy efficiency, and minimum entropy generation.

2 HT-CAES Thermodynamic Cycle

Figure 1 represents the HT-CAES thermodynamic cycles that are analyzed here. In the hybrid system, a portion of the available energy is stored in the form of compressed air and the remainder is converted directly to heat through Joule/resistive heating and is stored in a thermal energy storage (TES) unit. The TES unit is an inexpensive, solid-state, and sensible storage medium with high specific heat. As such, the TES is capable of high operating temperatures, with a limit dictated by its material properties. An alumina-based refractory is capable of operating temperatures in excess of ~1700 K, and resistive heating through Nichrome wires can provide continuous operating temperatures of ~1680 K [38]. The high-temperature capability associated with resistive heating and storage shifts the capacity of the system toward thermal storage, which has the potential of drastically reducing the storage pressures and volumes without a compromise in energy density.

The thermodynamic models assume an adiabatic and constant pressure air storage, which can be either underwater air storage or a cavern constructed in an underground rock formation with a water-equalizing pit to maintain isobaric conditions [55]. Air storage under this assumption remains isothermal and therefore reduces to just a delay time in the operation of the plant. Figures 1(a) and 1(b) show the described HT-CAES system with and without regeneration.

The sensible TES unit, shown in Fig. 1, is inherently a transient component that reaches maximum temperature, $T_{\max}$, at peak charge and minimum temperature, $T_{\min}$, culminating the discharge process. However, the TES can be designed to deliver a constant temperature, necessary for the optimal operation of an expander, by bypassing a portion of the cold inlet air with the hot flow exiting the TES, as demonstrated by Fig. 1. The TES is designed with minimum temperature, T_{min}, that is equivalent to the constant turbine inlet temperature, and higher than the compressor exhaust temperature ($T_{min} = T_3$ in the case without regeneration in Fig. 1(a), and $T_{min} = T_4$ with regeneration in Fig. 1(b)). The TES is assumed to be well mixed and absent of temperature gradients during charge and discharge. However, thermal storage efficiency is considered, and its value represents the percentage of irretrievable energy loss within a full cycle. Moreover, the analysis assumes a calorically perfect and ideal gas, with negligible pipe pressure drops.

3 Internally Reversible HT-CAES

We first consider an internally reversible HT-CAES system *without* regeneration in Sec. 3.1, followed by a similar analysis *with* regeneration in Sec. 3.2. In addition to internal reversibility, this section also assumes that the TES is 100% energy efficient. In Sec. 4, the TES efficiency along with internal irreversibilities is analyzed. The following analysis provides a formulation of the energy efficiency, exergy efficiency, and entropy generation as functions of the pressure ratio—where the pressure ratio is defined as the maximum-to-minimum pressure ratio of the system ($r = P_2/P_1 = P_3/P_4$ in Fig. 1(a)).

3.1 HT-CAES Without Regeneration

3.1.1 First Law Efficiency. The roundtrip energy storage efficiency of the HT-CAES system, defined as the output power over the total input power, is given by the following equation:

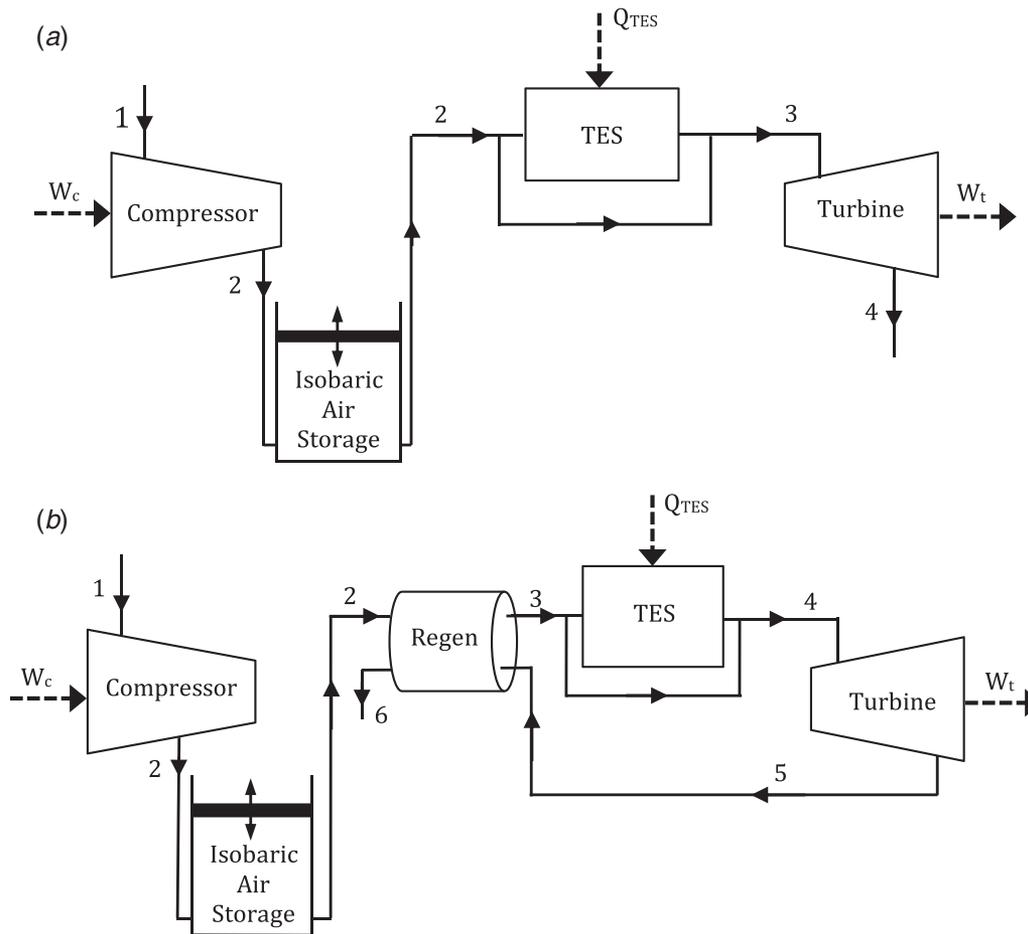$$\eta_I = \frac{\dot{W}_t}{\dot{W}_C + \dot{Q}_{\text{TES}}} \tag{1}$$

Fig. 1 HT-CAES thermodynamic cycle configuration (a) without and (b) with regeneration

Assuming constant specific heats for air, isentropic compressor and turbine, and constant turbine inlet temperature T_3, in Fig. 1(a), the energy efficiency can be rewritten as Eq. (2):

$$\eta_I = \frac{1 - T_1/T_2}{1 - T_1/T_3} = \frac{1 - r^{-\alpha}}{1 - r_T^{-1}} \tag{2}$$

where $\alpha = (\gamma - 1)/\gamma$, γ is the ratio of specific heats for air, and r_T is the maximum-to-minimum temperature ratio in the cycle ($r_T = \frac{T_3}{T_1}$ in Fig. 1(a)). By examining Eq. (2) and considering a Brayton cycle with a heat source provided by the TES, it becomes evident that the numerator represents the Brayton cycle efficiency in the case of pure thermal energy storage and no air storage. Similarly, the denominator of Eq. (2) represents the Carnot efficiency. Therefore, Eq. (2) can be written as Eq. (3):

$$\eta_I = \frac{\eta_{\text{Brayton}}}{\eta_{\text{Carnot}}} \tag{3}$$

Equation (3) provides an interesting result illustrating that the process has a perfect energy retrieval when no heat is added by the thermal storage. In such a case, the hybrid system is a mere advanced adiabatic design, with compression and expansion occurring along the same isentrope. As a result, the system is not bound by the Carnot limit. Moreover, with the addition of heat through the TES, the hybrid system efficiency remains higher than its associated Brayton cycle counterpart [33].

3.1.2 Second Law Efficiency. The roundtrip exergy efficiency of the HT-CAES system, which is defined as the ratio of total output to input exergy, is given by Eq. (4):

$$\eta_{II} = \frac{\int \dot{W}_t dt}{\int \dot{W}_c dt + \int (1 - T_1/T_{\text{TES}}) \dot{Q}_{\text{TES}} dt} \tag{4}$$

where $\dot{Q}_{\text{TES}}$ is the TES input Joule heating power. The total energy stored in the TES is calculated through an energy balance that results in $Q_{\text{TES}} = \dot{Q}_{\text{TES}} t Mc(T_{max} - T_{min}) = Mc(T_{max} - T_3) = \dot{m}c_p t(T_3 - T_2)$, where M, c, $\dot{m}$, and c_p are the TES mass, TES-specific heat, air mass flow rate, and specific heat of air at constant pressure, respectively. Lastly, the instantaneous temperature of the TES during the charge process is calculated through an energy balance, which results in $T_{\text{TES}} = \frac{\dot{Q}_{\text{TES}}}{Mc} t + T_{min}$, where $T_{min} = T_3$. Evaluating the integrals in Eq. (4) results in Eq. (5):

$$\eta_{II} = \frac{T_3 - T_4}{T_2 - T_1 + \frac{Mc}{\dot{m}c_p t}(T_{max} - T_3) - T_1 \frac{Mc}{\dot{m}c_p t} \ln\left(\frac{T_{max}}{T_3}\right)} \tag{5}$$

Further simplification of Eq. (5), substituting temperature ratios $r_T = \frac{T_3}{T_1}$ and $r_H = \frac{T_{max}}{T_3}$, leads to Eq. (6):

$$\eta_{II} = \frac{\eta_{\text{Brayton}}}{\eta_{\text{Carnot}} - r_T^{-1}(1 - r_T^{-1}r^\alpha) \frac{\ln(r_H)}{(r_H - 1)}} \tag{6}$$

The equation reveals that the exergy efficiency of the HT-CAES system is always higher than its energy efficiency given by Eq. (3), provided that the TES increases the temperature of the discharging air, $T_2 < T_3$. This result is consistent with heat engines, in which their exergy efficiencies are generally higher than their associated energy efficiencies.

3.1.3 Entropy Generation. The total entropy generation associated with the operation of the HT-CAES system is evaluated through an entropy balance and is given in Eq. (7):

$$S_{gen} = \int \frac{\dot{Q}_{out}}{T_{out}} dt - \int \frac{\dot{Q}_{in}}{T_{in}} dt \qquad (7)$$

The second integral in Eq. (7), associated with the TES heat input, is calculated through a similar approach that arrived at Eq. (5), resulting in the following expression:

$$S_{gen} = \frac{\dot{m}c_P t(T_4 - T_1)}{T_1} - Mc\ln\left(\frac{T_{max}}{T_3}\right) \qquad (8)$$

Normalizing the entropy generation with the total stored air mass times its specific heat, $\dot{m}c_P t$, and relating temperature ratios to pressure ratios through isentropic relations, results in Eq. (9):

$$\frac{S_{gen}}{\dot{m}c_P t} = (r_T r^{-\alpha} - 1) + (r_T^{-1} r^\alpha - 1)\frac{\ln(r_H)}{r_H - 1} \qquad (9)$$

Finally, plotting the energy efficiency, exergy efficiency, and normalized entropy generation given by Eqs. (3), (6), and (9), respectively, results in Fig. 2.

In the case of an internally reversible HT-CAES system without regeneration, all performance indices monotonically improve by increasing the operating pressure, as shown by Fig. 2. Therefore, in this specific case, an increase in the energy and exergy efficiency does, in fact, correlate with a decrease in the entropy generation. It is also imperative to note that in an HT-CAES system, the output power increases with the pressure ratio as the turbine and compressor are decoupled, in contrast to a Brayton cycle. Therefore, a decrease in the entropy generation also correlates with an increase in the output power. In Sec. 4, it will be shown that this is not necessarily the case in the presence of internal irreversibilities, and a discussion explaining the reason for the phenomenon is provided in Sec. 5.

3.2 HT-CAES With Regeneration. Undertaking a similar procedure, we arrive at the energy efficiency, exergy efficiency, and entropy generation for the case of an internally reversible HT-CAES system with regeneration (Fig. 1(b)). Similarly, the
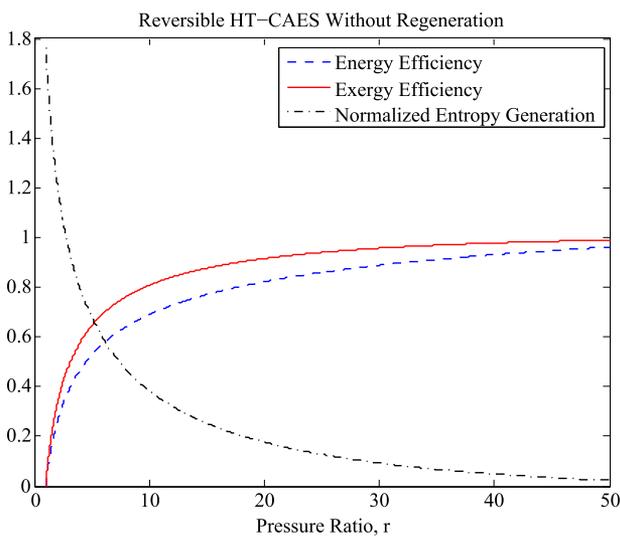

Fig. 2 Energy efficiency, exergy efficiency, and normalized entropy generation of the internally reversible HT-CAES system without regeneration as a function of the pressure ratio, *r*, assuming a 100% energy-efficient TES

pressure ratio is varied, and the performance indices are examined and compared to determine whether the minimization of entropy production correlates with energy and exergy losses.

3.2.1 First Law Efficiency. The energy efficiency, as defined in Eq. (1) and assuming constant specific heat, leads to Eq. (10):

$$\eta_I = \frac{T_4 - T_5}{T_2 - T_1 + T_4 - T_3} \qquad (10)$$

Rearranging Eq. (10) and relating temperature ratios to pressure ratios through isentropic relations leads to Eq. (11):

$$\eta_I = \frac{1}{2 - \eta_{\text{Brayton},R}} \qquad (11)$$

where $\eta_{\text{Brayton},R}$ is the energy efficiency of the corresponding regenerative Brayton cycle (Eq. 12) in the case of pure TES and no air storage. Equation (11) is analogous to Eq. (3); however, it includes regeneration:

$$\eta_{\text{Brayton},R} = 1 - r_T^{-1} r^\alpha \qquad (12)$$

The temperature ratios $r_T = \frac{T_4}{T_1}$ and $r_H = \frac{T_{max}}{T_4}$ are defined as the maximum-to-minimum temperature ratios that the air and TES experience during the regenerative cycle. Equation (11) illustrates that the first law efficiency of a regenerative HT-CAES system is always higher than its Brayton cycle counterpart, as was the case in the non-regenerative system shown by Eq. (3) [33].

3.2.2 Second Law Efficiency. The second law efficiency of the HT-CAES system with regeneration (Fig. 1(b)) is obtained through a similar procedure that arrived at the exergy efficiency without regeneration given by Eq. (6). The result is given by Eq. (13):

$$\eta_{II} = \frac{\eta_I}{1 - \eta_I \dfrac{\ln(r_H)}{r_T(r_H - 1)}} \qquad (13)$$

where η_I is the first law efficiency given by Eq. (11). Through an energy balance, the following relation given by Eq. (14) was used to relate the mass and specific heats of the air and TES with their temperature differences:

$$\frac{Mc}{\dot{m}c_P t} = \frac{T_4 - T_3}{T_{max} - T_4} = \frac{(1 - r^{-\alpha})}{r_H - 1} \qquad (14)$$

Again, notice that the second law efficiency of the HT-CAES system, given by Eq. (13), is always higher than its first law efficiency. The gap between energy and exergy efficiency increases with increasing energy efficiency and decreasing temperature ratios (r_T and r_H). This means that it is more exergetically effective to reduce the TES and air-temperature changes throughout the cycle as a result of the associated decrease in mixing irreversibilities.

3.2.3 Entropy Generation. The normalized entropy generation associated with the regenerative HT-CAES system, Fig. 1(b), is evaluated through an entropy balance given by Eq. (7). Undertaking a similar procedure that arrived at Eq. (9) results in Eq. (15):

$$\frac{S_{gen}}{\dot{m}c_P t} = (r^\alpha - 1) + (r^{-\alpha} - 1)\frac{\ln(r_H)}{r_H - 1} \qquad (15)$$

Finally, plotting the energy efficiency, exergy efficiency, and the normalized entropy generation given by Eqs. (11), (13), and (15) results in Fig. 3.

In the case of an internally reversible HT-CAES system with regeneration, the optimum operating pressure occurs at unity, as measured by the maximum energy and exergy efficiencies along with the coincident minimum entropy generation. However, at a pressure ratio of unity, the power output is zero. Therefore, to
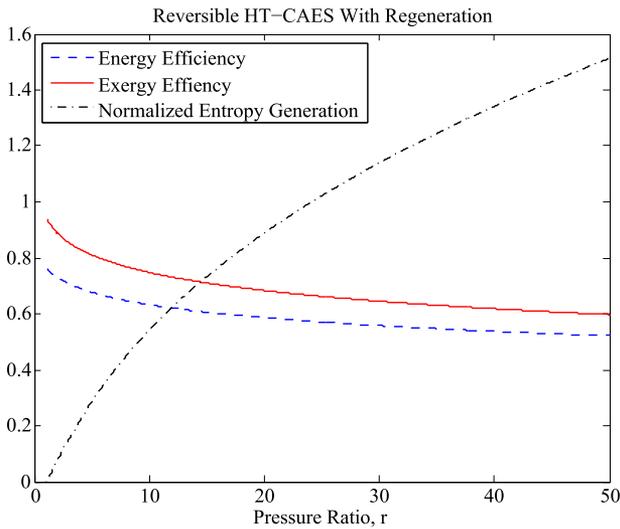
Fig. 3 Energy efficiency, exergy efficiency, and normalized entropy generation of the internally reversible HT-CAES system with regeneration as a function of the pressure ratio, r, assuming 100% energy-efficient TES

achieve finite time processes, and for the system to become operational, entropy must be generated. This contradicts the Gouy-Stodola theorem of heat engines, which demonstrates that maximum output power correlates with minimum entropy generation. In Sec. 4, internal irreversibilities and TES efficiencies are considered to determine whether minimization of entropy generation may lead to conclusive design guidelines in a real system.

4 Internally Irreversible HT-CAES With Regeneration

We now consider the regenerative HT-CAES system (Fig. 1(b)) with the presence of internal irreversibilities and TES inefficiency. The analysis is similar to the procedures involved in the reversible case, Sec. 3.2. However, the temperatures T_2, T_5, T_3, and T_6 need to be determined as functions of other operating parameters. Using isentropic component efficiencies, regenerator effectiveness, and an energy balance of the regenerator results in the following temperatures corresponding to Fig. 1(b):

$$T_2 = T_1\left(1 + \frac{1}{\eta_c}(r^\alpha - 1)\right) \tag{16}$$

$$T_5 = T_4(1 - \eta_T(1 - r^{-\alpha})) \tag{17}$$

$$T_3 = T_2 + (T_5 - T_2)\eta_R \tag{18}$$

$$T_6 = T_5 + T_2 - T_3 \tag{19}$$

where η_c, η_T, and η_R are the compressor, turbine, and regenerator efficiencies, respectively.

4.1 First Law Efficiency.
Starting with Eq. (1) and undertaking a similar procedure that arrived at Eqs. (3) and (11) results in Eq. (20), where η_H is the TES efficiency:

$$\eta_I = \frac{T_4 - T_5}{T_2 - T_1 + (T_4 - T_3)/\eta_H} \tag{20}$$

Using temperatures (16) through (19) results in Eq. (21):

$$\eta_I = \frac{\eta_T\eta_H\eta_C(1 - r^{-\alpha})}{(\eta_H + \eta_R - 1)\,r_T^{-1}(r^\alpha - 1) + \eta_C\eta_R\eta_T(1 - r^{-\alpha}) + \eta_{\text{Carnot}}\eta_C(1 - \eta_R)} \tag{21}$$

where η_{Carnot} is the Carnot efficiency of the corresponding the Brayton cycle, analogous to the HT-CAES cycle of Fig. 1(b), and provided by Eq. (22):

$$\eta_{\text{Carnot}} = 1 - \frac{T_1}{T_4} = 1 - r_T^{-1} \tag{22}$$

We can find an optimum compression ratio that would result in a maximum energy efficiency by applying $(\partial\eta_I/\partial r) = 0$, whose solution results in Eq. (23):

$$r_{opt}(\eta_{I,max}) = \left(1 + \sqrt{\frac{r_T\eta_C(1 - \eta_R)\eta_{\text{Carnot}}}{(\eta_R + \eta_H - 1)}}\right)^{\frac{1}{\alpha}} \tag{23}$$

Interestingly, the optimum pressure ratio that leads to maximum energy efficiency is independent of the turbine isentropic efficiency. In addition, when the regenerator effectiveness is unity, the optimum pressure ratio is also unity, coinciding with that of Fig. 3.

4.2 Second Law Efficiency.
Starting with Eq. (4) and undertaking a similar procedure that arrived at Eqs. (6) and (13) results in Eq. (24):

$$\eta_{II} = \frac{T_4 - T_5}{T_2 - T_1 + \dfrac{Mc}{\dot{m}c_p t}(T_{max} - T_4) - T_1\dfrac{Mc}{\dot{m}c_p t}\ln\left(\dfrac{T_{max}}{T_4}\right)} \tag{24}$$

where the mass and specific heats of the air and TES medium are related by Eq. (25):

$$\frac{Mc}{\dot{m}c_P t} = \frac{T_4 - T_3}{\eta_H(T_{max} - T_4)} \tag{25}$$

Substituting Eqs. (16) through (19) and Eq. (25) into Eq. (24) and simplifying results in Eq. (26)

$$\eta_{II} = \frac{\eta_T\eta_H\eta_C(1 - r^{-\alpha})}{(r^\alpha - 1)r_T^{-1}(\eta_H - A + A\eta_R) + A\eta_T\eta_C\eta_R(1 - r^{-\alpha}) + \eta_{\text{Carnot}}A\eta_C(1 - \eta_R)} \tag{26}$$

where

$$A = 1 - \frac{\ln(r_H)}{r_T(r_H - 1)} \tag{27}$$

We can find an optimum compression ratio that would result in the maximum exergy efficiency by applying $(\partial\eta_{II}/\partial r) = 0$, whose solution results in Eq. (28):

$$r_{opt}(\eta_{II,\text{max}})$$
$$= \left(1 + \sqrt{\frac{\eta_C(1 - \eta_R)\eta_{\text{Carnot}}[r_T(r_H - 1) - \ln(r_H)]}{(r_H - 1)(\eta_R + \eta_H - 1) + (1 - \eta_R)r_T^{-1}\ln(r_H)}}\right)^{\frac{1}{\alpha}} \tag{28}$$

Similar to the optimum pressure ratio leading to maximum energy efficiency, Eq. (23), the optimum pressure ratio that leads to the maximum exergy efficiency is independent of the turbine isentropic efficiency. In addition, when the regenerator effectiveness is unity, the optimum pressure ratio is also unity, coinciding with that of Fig. 3.

4.3 Entropy Generation.

Starting with Eq. (7) and undertaking a similar procedure that arrived at Eqs. (9) and (15)—however, with an additional heat-loss term associated with the TES efficiency—results in Eq. (29):

$$\frac{S_{gen}}{\dot{m}c_p t} = \left(\frac{T_6}{T_1} - 1\right) - \frac{T_4 - T_3}{\eta_H(T_{max} - T_4)}\ln\left(\frac{T_{max}}{T_4}\right) \\ + \frac{2(T_4 - T_3)(1 - \eta_H)/\eta_H}{T_{max}(1 + \eta_H) + T_4(1 - \eta_H)} \quad (29)$$

Using the temperatures in Eqs. (16) through (19) and finding an optimum compression ratio that would result in the minimum entropy generation by applying $(\partial S_{gen}/\partial r) = 0$ results in Equation (30):

$$r_{opt}(S_{gen,min}) = \left(\frac{\eta_T\eta_H\eta_C(1 - \eta_R)r_T + \eta_C\eta_T\eta_R B}{\eta_R\eta_H + r_T^{-1}(1 - \eta_R)B}\right)^{1/2\alpha} \quad (30)$$

where

$$B = \frac{\ln(r_H)}{r_H - 1} - \frac{2}{r_H((1 + \eta_H)/(1 - \eta_H)) + 1} \quad (31)$$

Typical trends of the energy efficiency, exergy efficiency, and normalized entropy generation as functions of the pressure ratio, given by Eqs. (21), (26), and (29), are illustrated in Fig. 4.

The results provided in Fig. 4 represent the case with the following efficiencies: $\eta_R = 0.6$, $\eta_c = \eta_T = \eta_H = 0.9$, $r_T = 3.33$, and $r_H = 1.5$. In contrast to a Brayton cycle, the compressor is decoupled from the turbine in the HT-CAES system and the turbine power is entirely available for useful work. Therefore, the power output increases monotonically with the increasing pressure ratio. Consequently, Fig. 4 offers a design region in terms of the pressure ratio: the pressure ratio of a real HT-CAES system should be larger than $r(\eta_{I,max})$. The rationale is that the system efficiency should only be compromised for higher output power, depending on the specific applications of use and their priorities, e.g., cost, size, or performance. Figure 4 reveals that the operational regime at minimum entropy generation is different from that at maximum exergy efficiency, maximum energy efficiency, and maximum work output. This indicates that a real HT-CAES system design based on a minimum entropy generation criterion would, in general, not operate at maximum work output, maximum energy efficiency, or maximum exergy efficiency. It will be further shown in a forthcoming

discussion that under certain conditions, the regime of minimum entropy generation becomes equivalent to the regime of maximum energy and exergy efficiency.

The optimum pressure ratios corresponding to the maximum energy efficiency, maximum exergy efficiency, and minimum entropy generation, given by Eqs. (23), (28), and (30), are plotted as a function of the regenerator effectiveness in Fig. 5. The results shown in Fig. 5 are plotted assuming $\eta_c = \eta_T = \eta_H = 0.9$, $r_T = 3.33$, and $r_H = 1.5$. Figure 5 reveals that the design regime corresponding to minimum entropy generation occurs at a lower-pressure ratio than that which corresponds to maximum energy efficiency and maximum exergy efficiency—more specifically, $r(S_{gen,min}) < r(\eta_{II,max}) < r(\eta_{I,max})$. In addition, as the regenerator effectiveness decreases, the optimum pressure ratios corresponding to all performance indices increase, and their differences also increase. As evident by Eqs. (23) and (28) and their plots in Fig. 5, the optimum pressure ratio leading to maximum energy and exergy efficiencies, at regenerator effectiveness of unity, is unity. Moreover, the optimum pressure ratio corresponding to minimum entropy generation, at $\eta_R = 1$ and as given by Eq. (30), leads to a calculated value of 0.49, which is a nonoperational value. However, restricting the pressure ratios to values above unity results in an optimum of unity. Therefore, at a regenerator effectiveness of unity, all optimum design conditions converge, which is in agreement with the reversible case, as given by Fig. 3. In contrast, a regenerator effectiveness of 0.5 leads to a convergence in the optimum pressure ratios, leading to maximum output power, maximum energy efficiency, and minimum entropy generation in a Brayton cycle [54].

A plot of the optimum pressure ratios as a function of the temperature ratio, r_T, is given in Fig. 6 for $\eta_R = \eta_c = \eta_T = \eta_H = 0.9$ and $r_H = 1.5$. Figure 6 further demonstrates that optimum design criteria do not necessarily coincide. More specifically, as in the case with varying regenerator effectiveness, the following holds: $r(S_{gen,min}) < r(\eta_{II,max}) < r(\eta_{I,max})$. The effect of TES efficiency on the optimum pressure ratio design is illustrated by Fig. 7, assuming $\eta_R = \eta_c = \eta_T = 0.9$, $r_H = 1.5$, and $r_T = 3.33$ for all performance indices, given by Eqs. (23), (28), and (30). The optimum pressure ratio, for all indices, increases with decreasing thermal storage efficiency. Additionally, Fig. 6 reveals that the optimum pressure is again observed in the same order, $r(S_{gen,min}) < r(\eta_{II,max}) < r(\eta_{I,max})$, as that in Figs. 5 and 6. Figure 7 illustrates that the optimum pressure ratio values corresponding to the minimum entropy generation at TES efficiencies
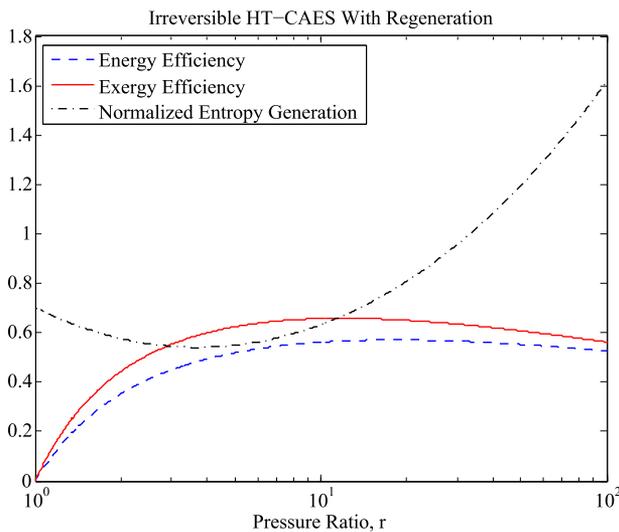

Fig. 4 Energy efficiency, exergy efficiency, and normalized entropy generation of the regenerative HT-CAES cycle corresponding to Fig. 1(b), with $\eta_R = 0.6$, $\eta_c = \eta_T = \eta_H = 0.9$, $r_T = 3.33$, and $r_H = 1.5$
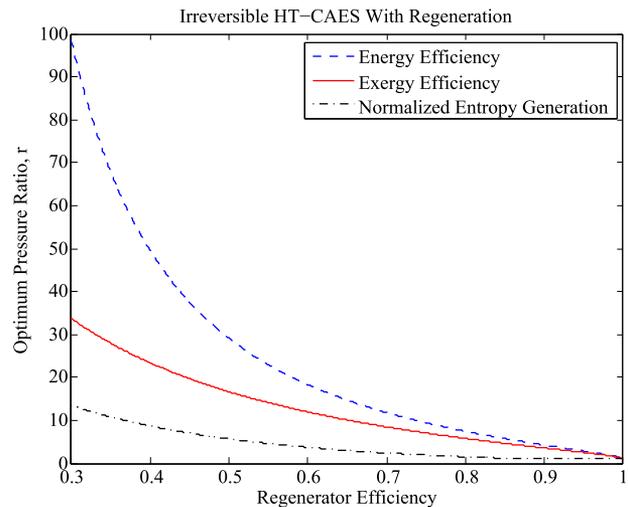

Fig. 5 The optimum pressure ratios corresponding to maximum energy efficiency, maximum exergy efficiency, and minimum normalized entropy generation of the regenerative HT-CAES cycle, corresponding to Fig. 1(b), as the regenerator effectiveness is varied, with $\eta_c = \eta_T = \eta_H = 0.9$, $r_T = 3.33$, and $r_H = 1.5$
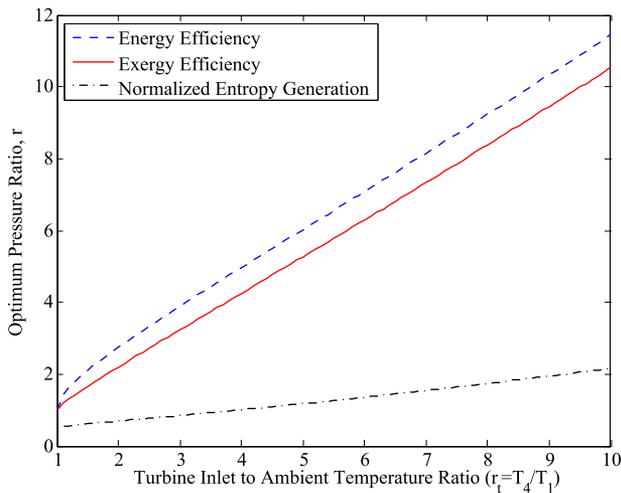
Fig. 6   The optimum pressure ratios corresponding to maximum energy efficiency, maximum exergy efficiency, and minimum normalized entropy generation of the regenerative HT-CAES cycle, corresponding to Fig. 1(b), as the turbine inlet to the ambient temperature ratio is varied, with $\eta_R = \eta_c = \eta_T = \eta_H = 0.9$ and $r_H = 1.5$

Fig. 8   The optimum pressure ratios corresponding to maximum energy efficiency, maximum exergy efficiency, and minimum normalized entropy generation of the regenerative HT-CAES cycle, corresponding to Fig. 1(b), as the compressor isentropic efficiency is varied, with $\eta_R = \eta_H = \eta_T = 0.9$, $r_H = 1.5$, and $r_T = 3.33$

greater than 50% are below unity, which is nonoperational. Therefore, restricting Eq. (30) to operational values results in optimum pressure values of unity for TES efficiencies greater than 50%.

Lastly, the compressor isentropic efficiency is varied, and its effects on the optimal pressure ratios are investigated, as shown in Fig. 8, assuming $\eta_R = \eta_H = \eta_T$, $r_H = 1.5$, and $r_T = 3.33$. The trends exhibited by the optimal pressure ratios as the compressor isentropic efficiency is decreased in Fig. 8 are quite the opposite as those observed when the TES efficiency is decreased (Fig. 7). Nonetheless, the optimal pressure ratio ranking remains consistent, namely, $r(S_{gen,min}) < r(\eta_{II,max}) < r(\eta_{I,max})$. Equation (30) is again unbiased to the pressure ratio range. Therefore, although the optimum pressure ratio values corresponding to the minimum entropy generation are below unity, at compressor isentropic efficiencies less than 0.95, this indicates that the actual optimum and realistic value, although nonoperational, is in fact unity.
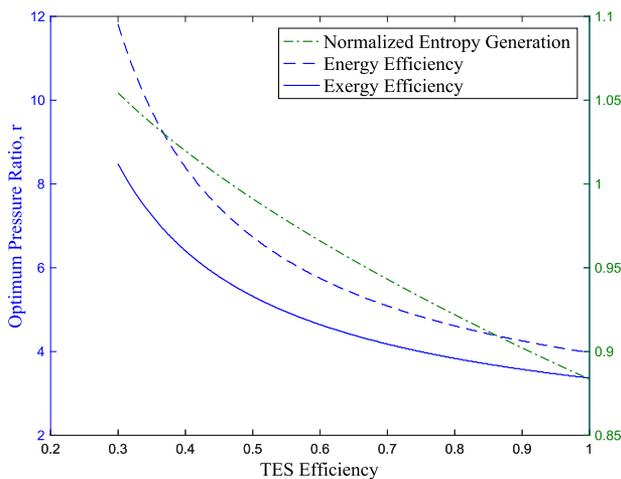

Fig. 7   The optimum pressure ratios corresponding to maximum energy efficiency, maximum exergy efficiency, and minimum normalized entropy generation of the regenerative HT-CAES cycle, corresponding to Fig. 1(b), as the TES efficiency is varied, with $\eta_R = \eta_c = \eta_T = 0.9$, $r_H = 1.5$, and $r_T = 3.33$
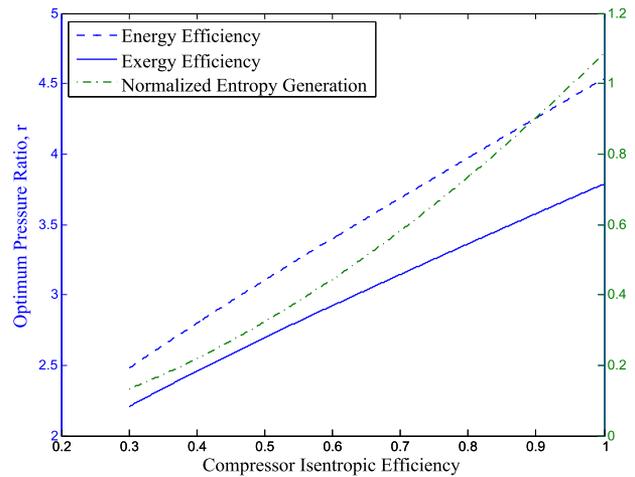
5   Discussion

The results of this work illustrate that it is inaccurate to generally interpret the generation of entropy as a measure of the energy and exergy losses in an HT-CAES system. The reason, as was demonstrated, is that the minimization of entropy generation generally does not correlate with the maximization of energy efficiency, exergy efficiency, or output power. As in the case of heat engines, it seems that the physical meaning of entropy generation is best described as "a measure of the dispersal of energy, or the tendency of energy to spread out in space" [28]. Therefore, the application of the second law of thermodynamics for the design of hybrid thermal and compressed air energy storage systems may not necessarily provide optimal energy utilization designs.

However, it is important to note that in certain conditions, the minimization of entropy generation may correlate with the maximization of energy efficiency, exergy efficiency, and power output. This was demonstrated in the case of an internally reversible and non-regenerative HT-CAES system, as shown in Fig. 2. In the case of an internally reversible and regenerative HT-CAES system, the maximum energy and exergy efficiency did correlate with the minimum entropy generation; however, they did not correlate with the maximum output power (Fig. 3). In practical applications, it is almost unavoidable to neglect internal irreversibilities, and the additional energy retrieval benefits provided by a regenerator far outweigh its costs. Therefore, representative results are better provided by the regenerative HT-CAES cycle with internal irreversibilities. In this case, minimum entropy generation coincides with maximum energy and exergy efficiencies and not with the maximum power when the regeneration is 100% effective. This is in contrast to heat engines, where optimum design conditions become coincident at a regenerator effectiveness of 50% [28]. It was also observed that the optimum pressure ratio corresponding to the minimum entropy generation generally occurs at lower values than those corresponding to maximum exergy and energy efficiencies. Furthermore, the following optimal pressure ratio order was consistently determined throughout the analysis: $r(S_{gen,min}) < r(\eta_{II,max}) < r(\eta_{I,max})$.

Further useful insights into the criteria necessary for coincident optimal design conditions can be obtained by combining the first and second laws of thermodynamics. Through the first law, the turbine output energy is given by Eq. (32):

$$W_T = W_C + Q_{in} - Q_{out} \qquad (32)$$

Eliminating Q_{out} from Eqs. (7) and (32) and dividing by the total input energy E_{input} results in Eq. (33):

$$\eta_I = 1 - \frac{T_1}{E_{input}}[Mcln(r_h) + S_{gen}] \tag{33}$$

Similarly, eliminating Q_{out} from Eqs. (7) and (32) and dividing by the total input exergy, $\mathbf{E}_{input}$, results in Eq. (34):

$$\eta_{II} = 1 - \frac{T_1}{\mathbf{E}_{input}}S_{gen} \tag{34}$$

The first and second law efficiencies, given by Eqs. (33) and (34), reveal the specific conditions that result in coincident minimum entropy generation and maximum energy and exergy efficiencies. As indicated by Eq. (33), the minimum entropy generation overlaps with the maximum energy efficiency only when the input energy, thermal energy storage mass, specific heat, and maximum-to-minimum temperature ratio, r_h, are a constant. Similarly, Eq. (34) reveals that minimum entropy generation coincides with the maximum exergy efficiency only if the total input exergy is a constant. Otherwise, the entire term in the vicinity of the entropy generation variable S_{gen} must reach a minimum for energy and exergy efficiencies to reach a maximum, in Eqs. (33) and (34).

6 Conclusion

A hybrid thermal and compressed air energy storage system is designed with an optimization objective of minimizing entropy generation. Internally reversible and irreversible assumptions were investigated, in addition to regenerative and non-regenerative designs. It is shown that a hybrid compressed air energy storage system designed based on this criterion may operate at an energy and exergy efficiency that is lower than the maximum possible achievable. The main conclusion is that the minimization of entropy generation does not necessarily correlate with the minimization of energy losses in a hybrid compressed air energy storage system. Only under certain circumstances does the minimum entropy generation coincide with maximum energy and exergy efficiencies. Moreover, the optimum operating pressure conditions based on maximum energy efficiency, maximum exergy efficiency, and minimum entropy generation are ordered in the following manner: $r(S_{gen,min}) < r(\eta_{II,max}) < r(\eta_{I,max})$.

Acknowledgment

Nomenclature

c = TES-specific Heat
r = pressure ratio
t = total charge or discharge time
M = TES mass
P = pressure
R = ideal gas constant of air
T = temperature
$\dot{m}$ = mass flow rate
$\dot{W}_c$ = compressor input power
$\dot{W}_t$ = turbine output power
c_p = specific heat of air at constant pressure
c_v = specific heat of air at constant volume
r_H = maximum TES temperature ratio
r_{opt} = optimum pressure ratio
r_T = maximum cycle temperature ratio
E_{input} = input energy
Q_{in} = input heat
Q_{out} = output heat
Q_{TES} = TES energy input
S_{gen} = entropy generation
W_c = compression energy
W_t = turbine energy output
$\mathbf{E}_{input}$ = input exergy
γ = ratio of specific heat for air
$\eta_{Brayton}$ = Brayton cycle efficiency
$\eta_{Brayton,R}$ = regenerative Brayton cycle efficiency
η_{Carnot} = Carnot efficiency
η_c = compressor isentropic efficiency
η_H = TES efficiency
η_R = regenerator effectiveness
η_T = turbine isentropic efficiency
η_I = HT-CAES roundtrip energy efficiency (first law efficiency)
η_{II} = HT-CAES roundtrip exergy efficiency (second law efficiency)

References

[1] Can, S., Bie, Z., and Zhang, Z., 2016, "A New Framework for the Wind Power Curtailment and Absorption Evaluation," Int. Trans. Electr. Energy Syst., 26(10), pp. 2134–2147.

[2] Li, C. B., Shi, H. Q., Cao, Y. J., Wang, J., Kuang, Y., Tan, Y., and Wei, J., 2015, "Comprehensive Review of Renewable Energy Curtailment and Avoidance: A Specific Example in China," Renewable Sustainable Energy Rev., 41, pp. 1067–1079.

[3] Zou, J., Rahman, S., and Lai, X., 2015, "Mitigation of Wind Output Curtailment by Coordinating With Pumped Storage and Increasing Transmission Capacity," 2015 IEEE Power & Energy Society General Meeting, Denver, CO, July 26–30.

[4] Waite, M., and Modi, V., 2016, "Modeling Wind Power Curtailment With Increased Capacity in a Regional Electricity Grid Supplying a Dense Urban Demand," Appl. Energy, 183, pp. 299–317.

[5] Wang, C. X., 2015, "Study of Unit Commitment Strategies in Combating Wind Curtailment in China," 4th International Conference on Energy and Environmental Protection (ICEEP 2015), Hebron, Palestine, Apr. 6–7, pp. 1137–1140.

[6] Fan, X. C., Wang, W. Q., Shi, R. J., and Li, F. T., 2015, "Analysis and Countermeasures of Wind Power Curtailment in China," Renewable Sustainable Energy Rev., 52, pp. 1429–1436.

[7] Upendra Roy, B. P., and Rengarajan, N., 2017, "Feasibility Study of an Energy Storage System for Distributed Generation System in Islanding Mode," ASME J. Energy Resour. Technol., 139(1), p. 011901.

[8] Koytsoumpa, E.-I., Bergins, C., Buddenberg, T., Wu, S., Sigurbjornsson, O., Tran, K. C., and Kakaras, E., 2016, "The Challenge of Energy Storage in Europe: Focus on Power to Fuel," ASME J. Energy Resour. Technol., 138(4), p. 042002.

[9] Herrmann, S., Kahlert, S., Wuerth, M., and Spliethoff, H., 2017, "Thermo-Economic Evaluation of Novel Flexible CAES/CCPP Concept," ASME J. Energy Resour. Technol., 139(1), p. 011902.

[10] Mazloum, Y., Sayah, H., and Nemer, M., 2016, "Static and Dynamic Modeling Comparison of an Adiabatic Compressed Air Energy Storage System," ASME J. Energy Resour. Technol., 138(6), p. 062001.

[11] Kushnir, R., Ullmann, A., and Dayan, A., 2012, "Thermodynamic Models for the Temperature and Pressure Variations Within Adiabatic Caverns of Compressed Air Energy Storage Plants," ASME J. Energy Resour. Technol., 134(2), p. 021901.

[12] Hameer, S., and van Niekerk, J. L., 2015, "A Review of Large-Scale Electrical Energy Storage," Int. J. Energy Res., 39(9), pp. 1179–1195.

[13] Freeman, E., Occello, D., and Barnes, F., 2016, "Energy Storage for Electrical Systems in the USA," Aims Energy, 4(6), pp. 856–875.

[14] Zakeri, B., and Syri, S., 2015, "Electrical Energy Storage Systems: A Comparative Life Cycle Cost Analysis," Renewable Sustainable Energy Rev., 42, pp. 569–596.

[15] Obi, M., Jensen, S. M., Ferris, J. B., and Bass, R. B., 2017, "Calculation of Levelized Costs of Electricity for Various Electrical Energy Storage Systems," Renewable Sustainable Energy Rev., 67, pp. 908–920.

[16] Yao, E., Wang, H., Wang, L., Xi, G., and Marechal, F., 2017, "Multi-Objective Optimization and Exergoeconomic Analysis of a Combined Cooling, Heating

[16] and Power Based Compressed Air Energy Storage System," Energy Convers. Manage., **138**, pp. 199–209.

[17] Ji, W., Zhou, Y., Sun, Y., Zhang, W., An, B., and Wang, J., 2017, "Thermodynamic Analysis of a Novel Hybrid Wind-Solar-Compressed Air Energy Storage System," Energy Convers. Manage., **142**, pp. 176–187.

[18] Sciacovelli, A., Li, Y., Chen, H., Wu, Y., Wang, J., Garvey, S., and Ding, Y., 2017, "Dynamic Simulation of Adiabatic Compressed Air Energy Storage (A-CAES) Plant With Integrated Thermal Storage—Link Between Components Performance and Plant Performance," Appl. Energy, **185**(1), pp. 16–28.

[19] Wolf, D., and Budt, M., 2014, "LTA-CAES—A Low-Temperature Approach to Adiabatic Compressed Air Energy Storage," Appl. Energy, **125**, pp. 158–164.

[20] Peng, H., Yang, Y., Li, R., and Ling, X., 2016, "Thermodynamic Analysis of an Improved Adiabatic Compressed Air Energy Storage System," Appl. Energy, **183**, pp. 1361–1373.

[21] Odukomaiya, A., Abu-Heiba, A., Gluesenkamp, K. R., Abdelaziz, O., Jackson, R. K., Daniel, C., Graham, S., and Momen, A. M., 2016, "Thermal Analysis of Near-Isothermal Compressed Gas Energy Storage System," Appl. Energy, **179**, pp. 948–960.

[22] Venkataramani, G., Parankusam, P., Ramalingam, V., and Wang, J., 2016, "A Review on Compressed Air Energy Storage—A Pathway for Smart Grid and Polygeneration," Renewable Sustainable Energy Rev., **62**, pp. 895–907.

[23] Garvey, S. D., and Pimm, A., 2016, "Compressed Air Energy Storage," *Storing Energy*, T. M. Letcher, ed., Elsevier, Oxford, pp. 87–111.

[24] Olabi, A. G., 2017, "Renewable Energy and Energy Storage Systems," Energy, **136**, pp. 1–6.

[25] Kilic, M., and Mutlu, M., 2016, "A Novel Design of a Compressed Air Storage System With Liquid Pistons," Bulg. Chem. Commun., **48**(Special Issue: E2), pp. 318–324.

[26] Li, P. Y., and Saadat, M., 2016, "An Approach to Reduce the Flow Requirement for a Liquid Piston Near-Isothermal Air Compressor/Expander in a Compressed Air Energy Storage System," IET Renewable Power Generation, **10**(10), pp. 1506–1514.

[27] Qin, C., and Loth, E., 2014, "Liquid Piston Compression Efficiency With Droplet Heat Transfer," Appl. Energy, **114**, pp. 539–550.

[28] Buhagiar, D., and Sant, T., 2017, "Modelling of a Novel Hydro-Pneumatic Accumulator for Large-Scale Offshore Energy Storage Applications," J. Energy Storage., **14**, pp. 283–294.

[29] Budt, M., Wolf, D., Span, R., and Yan, J., 2016, "A Review on Compressed Air Energy Storage: Basic Principles, Past Milestones and Recent Developments," Appl. Energy, **170**, pp. 250–268.

[30] Qin, C., and Loth, E., 2016, "Simulation of Spray Direct Injection for Compressed Air Energy Storage," Appl. Therm. Eng., **95**, pp. 24–34.

[31] McBride, T., Bell, A., and Kepshire, D., 2013, *ICAES Innovation: Foam-Based Heat Exchange*, Seabrook, TX.

[32] Houssainy, S., 2017, Hybrid Thermal and Compressed Air Energy Storage System (HT-CAES): Thermodynamic Analysis and Thermoeconomic Optimization. UCLA. ProQuest ID: Houssainy_ucla_0031D_ 16397. Merritt ID: ark:/13030/m56x46w6. https://escholarship.org/uc/item/4p40j6bz

[33] Houssainy, S., Janbozorgi, M., and Kavehpour, P., 2018, "Theoretical Performance Limits of an Isobaric Hybrid Compressed Air Energy Storage System," ASME J. Energy Resour. Technol., **140**(10), p. 101201.

[34] Houssainy, S., and Kavehpour, H. P., 2015, "Free-Surface Profile of Evaporative Liquids at the Vicinity of the Contact Line," J. Coat Technol. Res., **12**(5), pp. 863–867.

[35] Baghaei Lakeh, R., Villazana, I. C., Houssainy, S., Anderson, K. R., and Kavehpour, H., 2016, "Design of a Modular Solid-Based Thermal Energy Storage for a Hybrid Compressed Air Energy Storage System," International Conference on Energy Sustainability, 2, ASME 2016 Energy Storage Forum, Charlotte, NC, June 26–30.

[36] Houssainy, S., Baghaei Lakeh, R., and Kavehpour, H., 2016, "A Thermodynamic Model of a High Temperature Hybrid Compressed Air Energy Storage System for Grid Storage," International Conference on Energy Sustainability, 2, ASME 2016 Energy Storage Forum, Charlotte, NC, June 26–30.

[37] Ip, P. P., Houssainy, S., and Kavehpour, H., 2017, "Modeling of a Low Cost Thermal Energy Storage System to Enhance Generation From Small Hydropower Systems," ASME Power Conference, Charlotte, NC, June 26–30.

[38] Houssainy, S., Janbozorgi, M., Ip, P., and Kavehpour, P., 2018, "Thermodynamic Analysis of a High Temperature Hybrid Compressed Air Energy Storage (HTH-CAES) System," Renewable Energy, **115**, pp. 1043–1054.

[39] Houssainy, S., Janbozorgi, M., and Kavehpour, P., 2018, "Thermodynamic Performance and Cost Optimization of a Novel Hybrid Thermal-Compressed Air Energy Storage System Design," J. Energy Storage, **18**, pp. 206–217.

[40] Luo, X., Wang, J. H., Krupke, C., Wang, Y., Sheng, Y., Li, J., Xu, Y. J., Wang, D., Miao, S. H., and Chen, H. S., 2016, "Modelling Study, Efficiency Analysis and Optimisation of Large-Scale Adiabatic Compressed Air Energy Storage Systems With Low-Temperature Thermal Storage," Appl. Energy, **162**, pp. 589–600.

[41] Cardenas, B., Pimm, A. J., Kantharaj, B., Simpson, M. C., Garvey, J. A., and Garvey, S. D., 2017, "Lowering the Cost of Large-Scale Energy Storage: High Temperature Adiabatic Compressed Air Energy Storage," Propulsion Power Res., **6**(2), pp. 126–133.

[42] de Biasi, V., 2009, "Fundamental Analyses to Optimize Adiabatic CAES Plant Efficiencies," Gas Turbine World, **134**(26e), p. 28.

[43] Doetsch, C., Budt, M., Wolf, D., and Kanngießer, A., 2012, Adiabates Niedertemperatur-Druckluftspeicherkraftwerk zur Unterstützung der Netzintegration von Windenergie, p. 0325211.

[44] Barbour, E., Mignard, D., Ding, Y., and Li, Y., 2015, "Adiabatic Compressed Air Energy Storage With Packed Bed Thermal Energy Storage," Appl. Energy, **155**, pp. 804–815.

[45] Dreißigacker, V., Zunft, S., and Müller-Steinhagen, H., 2013, "A Thermo-Mechanical Model of Packed-Bed Storage and Experimental Validation," Appl. Energy, **111**, pp. 1120–1125.

[46] Pirouz Kavehpour, H., Aryafar, H., Thacker, A., Janbozorgi, M., Houssainy, S., and Ismail, W., 2017, "The Regents of the University of California, Low-Cost Hybrid Energy Storage System," U.S. Patent No. WO2017044658 A1, Mar. 16, 2017.

[47] Yang, Z., Wang, Z., Ran, P., Li, Z., and Ni, W., 2014, "Thermodynamic Analysis of a Hybrid Thermal-Compressed Air Energy Storage System for the Integration of Wind Power," Appl. Therm. Eng., **66**(1–2), pp. 519–527.

[48] Mahdi Naserian, M., Farahat, S., and Sarhaddi, F., 2017, "New Exergy Analysis of a Regenerative Closed Brayton Cycle," Energy Convers. Manage., **134**, pp. 116–124.

[49] Sciacovelli, A., Verda, V., and Sciubba, E., 2015, "Entropy Generation Analysis as a Design Tool—A Review," Renewable Sustainable Energy Rev., **43**, pp. 1167–1181.

[50] Bejan, A., 1996, "Entropy Generation Minimization: The New Thermodynamics of Finite-Size Devices and Finite-Time Processes," J. Appl. Phys., **79**(3), pp. 1191–1218.

[51] Jafari, M., Parhizkar, M. J., Amani, E., and Naderan, H., 2016, "Inclusion of Entropy Generation Minimization in Multi-Objective CFD Optimization of Diesel Engines," Energy, **114**, pp. 526–541.

[52] Ge, Y., Chen, L., and Sun, F., 2008, "Finite-Time Thermodynamic Modelling and Analysis of an Irreversible Otto-Cycle," Appl. Energy, **85**(7), pp. 618–624.

[53] Haseli, Y., 2013, "Optimization of a Regenerative Brayton Cycle by Maximization of a Newly Defined Second Law Efficiency," Energy Convers. Manage., **68**, pp. 133–140.

[54] Haseli, Y., 2013, "Performance of Irreversible Heat Engines at Minimum Entropy Generation," Appl. Math. Model., **37**(23), pp. 9810–9817.

[55] Pimm, A., and Garvey, S. D., 2016, "Underwater Compressed Air Energy Storage," *Storing Energy*, T. M. Letcher, ed., Elsevier, Oxford, pp. 135–154.